

# CrystEngComm

Accepted Manuscript



This is an *Accepted Manuscript*, which has been through the Royal Society of Chemistry peer review process and has been accepted for publication.

*Accepted Manuscripts* are published online shortly after acceptance, before technical editing, formatting and proof reading. Using this free service, authors can make their results available to the community, in citable form, before we publish the edited article. We will replace this *Accepted Manuscript* with the edited and formatted *Advance Article* as soon as it is available.

You can find more information about *Accepted Manuscripts* in the [Information for Authors](#).

Please note that technical editing may introduce minor changes to the text and/or graphics, which may alter content. The journal's standard [Terms & Conditions](#) and the [Ethical guidelines](#) still apply. In no event shall the Royal Society of Chemistry be held responsible for any errors or omissions in this *Accepted Manuscript* or any consequences arising from the use of any information it contains.

## ARTICLE

# Polyoxometalate-Based Metal-Organic Coordination Networks for Heterogeneous Catalytic Desulfurization

Cite this: DOI: 10.1039/x0xx00000x

Received 00th January 20xx,  
Accepted 00th January 20xx

DOI: 10.1039/x0xx00000x

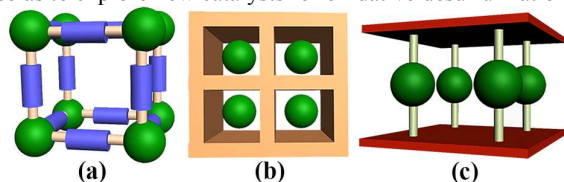
[www.rsc.org/](http://www.rsc.org/)Yuan-Yuan Ma,<sup>a</sup> Hua-Qiao Tan,<sup>\*a</sup> Yong-Hui Wang,<sup>a</sup> Xiu-Li Hao,<sup>\*ab</sup> Xiao-Jia Feng,<sup>ac</sup>  
Hong-Ying Zang,<sup>a</sup> and Yang-Guang Li<sup>\*a</sup>

Three new polyoxometalate (POM)-based metal-organic coordination networks (MOCNs) with the chemical formula of  $[\text{Co}(\text{BBTZ})_{1.5}(\text{HBBTZ})(\text{H}_2\text{O})_2][\text{PW}_{12}\text{O}_{40}]\cdot\text{H}_2\text{O}$  (**1**),  $[\text{Co}_{2.5}(\text{BBTZ})_4(\text{H}_2\text{O})_2][\text{BW}_{12}\text{O}_{40}]\cdot 4\text{H}_2\text{O}$  (**2**) and  $[\text{Cu}(\text{BBTZ})_2]_5[\text{BW}_{12}\text{O}_{40}]_2\cdot 4\text{H}_2\text{O}$  (**3**) (BBTZ = 1,4-bis-(1,2,4-triazol-1-ylmethyl)benzene) were hydrothermally synthesized in the reaction system containing Keggin-type POMs, transition metal salts (cobalt salts and copper salts) and BBTZ ligands. All compounds were characterized by elemental analyses, IR spectra, powder X-ray diffraction, TG analyses and single-crystal X-ray diffraction analyses. Compound **1** exhibits a POM-encapsulated 3-D supramolecular network, while compound **2** and **3** display the POM-supported 3-D coordination networks. Using oxidative desulfurization of dibenzothiophene (DBT) as the model, the catalytic activities of compounds **1-3** are investigated. All three compounds show efficient catalytic activity for oxidation of DBT with the order of  $\mathbf{2} > \mathbf{3} > \mathbf{1}$ . It is found that the POM species of compounds **1-3** play the main role in the catalytic oxidation desulfurization process, while the TM ions, the loading amount of POMs, and structural features of these POM-based MOCNs are also necessary factors to affect the catalytic activities. Furthermore, a surfactant-assisted hydrothermal synthesis method has been developed to prepare nanocrystal **2**. SEM reveals that the as-synthesized nanocrystallines **2** are about 245 nm. The catalytic oxidation desulfurization experiments show that nanocrystal **2** possesses much higher catalytic activities than those of large single crystal products of **2**.

## Introduction

The desulfurization of fossil fuels is a currently significant task, which is directly associated with the living environment of human beings.<sup>1</sup> In this research field, oxidative desulfurization has been considered as an effective strategy to remove refractory organosulfur substrates. To date, a key factor in this aspect is the exploration of new oxidative catalyst systems.<sup>2</sup> Polyoxometalates (POMs), as a unique metal-oxo clusters of early transition metals (such as Mo, W, V, Nb and Ta), have been proved one kind of most promising catalysts for desulfurization,<sup>3</sup> because of their excellent controllability in composition, structure, charge and redox properties at the molecular level. However, POMs sometimes show good solubility in the reaction system, and act as homogeneous catalysts with a poor recovery.<sup>4</sup> Furthermore, some POMs may suffer from a hydrolyzation in different pH of solution, which must be surmounted in the homogeneous system.<sup>5</sup> Moreover, the low specific surface area and the relatively low loading rate of POMs as heterogeneous catalysts also inhibit their catalytic applications.<sup>6</sup> Therefore, developing a new type of POMs-based catalytic materials with good stability, easy-recycling, high efficient catalytic activity is one of the currently challenging issues.

It is well known that metal-organic coordination networks (MOCNs) usually possess a good stability and relatively low solubility in solutions.<sup>7</sup> The introduction of POMs into MOCNs usually can not only load and disperse POM units into MOCNs at the molecular level, but also keep the redox activity of POM species well. Based on such consideration, a series of POM-based MOCNs have been constructed as the heterogeneous catalysts.<sup>8</sup> In these compounds, a few of them show good catalytic activities due to their porous structural features, which allow for the contact between reactants and the catalytic active sites (POMs).<sup>9</sup> In comparison with these limited porous compounds, numerous non-porous POM-based MOCNs have still been far unexplored as heterogeneous catalysts.<sup>10</sup> Thus, it is significant to develop new strategies to improve the catalytic activities of these non-porous hybrid compounds so as to explore new catalysts for oxidative desulfurization.

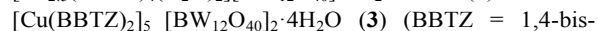
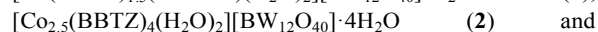
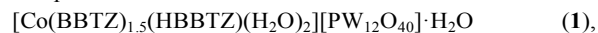


**Scheme 1** Schematic view of POM-based MOCNs in which POMs can act as (a) nodes, (b) templates, and (c) pillars (Green balls represent POM units).

Generally, POMs can act as nodes, templates and pillars (Scheme 1) in the POM-based MOCNs.<sup>11,12</sup> In any cases, a main concern is that how to introduce more POM units into the MOCN skeletons, and let them expose as much as possible in the reaction system. In this aspect, the combination of cationic MOCNs and various polyoxoanion

units is an effective way to maximize the loading amount of POMs. Following this strategy, we have constructed many POM-based cationic MOCNs by the hydrothermal reaction of polyoxoanions, transition metal (TM) cations and various neutral N-donor bridging ligands.<sup>13</sup> Although the loading amount of POMs in our previous work<sup>9b,13d</sup> have been significantly improved (about 71 %), their catalytic activities for oxidation desulfurization are still relatively low. The factors that affect the catalytic activity of these catalysts remain unexplored.

Herein, we report three new POMs-based cationic MOCN compounds:



(BBTZ = 1,4-bis-(1,2,4-triazol-1-ylmethyl) benzene). Using oxidative desulfurization of dibenzothiophene (DBT) as the model, we confirm that all three compounds exhibit effective catalytic activity for oxidation of DBT with the order of  $2 > 3 > 1$ . The effects of POMs, transition metal cations, the loading amount of POMs, and the structural features on the catalytic activities of compounds **1-3** have been investigated. Furthermore, a surfactant-assisted hydrothermal synthesis method is developed for the preparation of nanocrystalline compound **2** with high specific surface area. SEM reveals that the as-synthesized nanocrystallines **2** are about 245 nm, which exhibit much higher catalytic activities than those of large single crystal products of **2**.

## Experimental section

**Materials and methods** All reagents for syntheses were commercially purchased and used without further purification. The ligand 1,4-bis-(triazole-1-ylmethyl)benzene (BBTZ) was prepared according to the reported procedure.<sup>14</sup>  $\text{H}_3\text{PW}_{12}\text{O}_{40} \cdot n\text{H}_2\text{O}$  and  $\text{K}_3\text{BW}_{12}\text{O}_{40} \cdot n\text{H}_2\text{O}$  were prepared based on the literature methods.<sup>15</sup> Elemental analyses (C, H and N) were conducted on a Perkin-Elmer 2400 CHN elemental analyzer. W, Co and Cu were determined by a Leaman inductively coupled plasma (ICP) spectrometer. The IR spectra were recorded in the range of 4000-400  $\text{cm}^{-1}$  on an Alpha Centaur FT/IR spectrophotometer with pressed KBr pellets. The TG analyses were carried out under air flow by using a Pyris Diamond TG instrument at a heating rate of 10  $^\circ\text{C min}^{-1}$ . The powder X-ray diffraction (PXRD) patterns were collected by using a Rigaku D/max-IIIB X-ray diffractometer with Cu-K $\alpha$  ( $\lambda = 1.5418 \text{ \AA}$ ) radiation in the  $2\theta$  range of  $5^\circ$  to  $50^\circ$  at a scanning rate of  $1^\circ$  per minute. GC-MS spectra were obtained on an agilent 5875-6890N. The HPLC analyses were performed on a shimadazu LC-15C instrument.

## Synthesis



A mixture of  $\text{H}_3\text{PW}_{12}\text{O}_{40} \cdot n\text{H}_2\text{O}$  (0.6g, 0.2mmol),  $\text{Co}(\text{OAc})_2 \cdot 4\text{H}_2\text{O}$  (0.102g, 0.4mmol), and BBTZ (0.15g, 0.625mmol) was dissolved in 10 mL of distilled water at

room temperature and stirred for 0.5 h. The pH of the reaction mixture was adjusted to about 4.0 with 1.0 M NaOH. The suspension was sealed in a 23-mL Teflon-lined autoclave and heated at 140 °C for 3 days. After slow cooling to room temperature, brown block crystals were filtered and washed with distilled water (65 % yield based on W). Anal. Calcd for  $C_{30}H_{37}N_{15}O_{43}PW_{12}Co$ : C 10.02, H 1.03, N 5.85, W 61.45, Co 1.65; Found: C 10.22, H 1.09, N 5.64, W 61.39, Co 1.67. Selected IR (solid KBr pellet,  $cm^{-1}$ ): 3421(m), 3129(w), 1634(m), 1522(s), 1436(m), 1378(w), 1280(s), 1221(w), 1124(m), 1078(s), 975(s), 898(s), 804(s). TG analysis suggests that the first weight loss in the temperature range of 50 ~ 200 °C corresponds to the loss of three lattice and/or coordinated water molecules.

$[Co_{2.5}(BBTZ)_4(H_2O)_2][BW_{12}O_{40}] \cdot 4H_2O$  (2)

A mixture of  $K_5BW_{12}O_{40} \cdot n H_2O$  (0.4 g, 0.13 mmol),  $Co(OAc)_2 \cdot 4H_2O$  (0.102 g, 0.4 mmol), and BBTZ (0.15 g, 0.625 mmol) was dissolved in 10 mL of distilled water at room temperature and stirred for 0.5 h. The pH of the reaction mixture was adjusted to about 3.0 with 1.0 M HCl. The suspension was sealed in a 23-mL Teflon-lined autoclave and heated at 140 °C for 3 days. After slow cooling to room temperature, red-brown block crystals were filtered and washed with distilled water (78 % yield based on W). Anal. Calcd for  $C_{48}H_{60}N_{24}O_{46}BW_{12}Co_{2.5}$ : C 14.14, H 1.47, N 8.25, W 54.19, Co 3.62; Found: C 14.16, H 1.40, N 8.21, W 54.21, Co 3.48. Selected IR (solid KBr pellet,  $cm^{-1}$ ): 3413(s), 3124(w), 1617(m), 1527(s), 1426(m), 1352(w), 1278(s), 1216(w), 1135(s), 1017(m), 979(s), 924(s), 799(s). TG analysis suggests that the first weight loss in the temperature range of 50 ~ 210 °C corresponds to the loss of six lattice and/or coordinated water molecules.

$[Cu(BBTZ)_2]_5[BW_{12}O_{40}]_2 \cdot 4H_2O$  (3)

A mixture of  $K_5BW_{12}O_{40} \cdot n H_2O$  (0.4 g, 0.13 mmol),  $Cu(OAc)_2 \cdot H_2O$  (0.105g, 0.4 mmol), and BBTZ (0.15 g, 0.625 mmol) was dissolved in 10 mL of distilled water at room temperature and stirred for 0.5 h. The pH of the reaction mixture was adjusted to about 5.0 with 1.0 M NaOH. The suspension was sealed in a 23-mL Teflon-lined autoclave and heated at 140 °C for 3 days. After slow cooling to room temperature, blue block crystals were filtered and washed with distilled water (55 % yield based on W). Anal. Calcd for  $C_{120}H_{128}N_{60}O_{84}B_2W_{24}Cu_5$ : C 16.93, H 1.51, N 9.87, W 51.91, Cu 3.74; Found: C 16.96, H 1.53, N 9.82, W 51.95, Cu 3.78. Selected IR (solid KBr pellet,  $cm^{-1}$ ): 3436(s), 3108(s), 1621(w), 1525(s), 1424(m), 1352(w), 1280(s), 1129(s), 999(w), 950(s), 902(s), 821(s). TG analysis suggests that the first weight loss in the temperature range of 45 ~ 220 °C corresponds to the loss of four lattice water molecules.

### Preparation of nanocrystal of compound 2

The preparation of nanocrystalline compound 2 was similar to that of single crystal compound 2, except that the surfactant sodium dodecyl sulfate (SDS) (10 mg, 0.035 mmol) was added in the reaction system. The red-brown crystalline solid was filtered, washed with distilled water

and ethanol alternately, and dried in an oven at 60 °C for 24 h (70 % yield based on W). The nanocrystals with an average diameter of 245 nm were obtained based on the SEM images (Fig 8). The nanocrystals were characterized by FT/IR spectroscopy (Fig. S20†), PXRD (Fig. 11 and S19†), and EDX (Fig S23†).

### The procedure for catalytic oxidative desulfurization

The catalytic oxidation desulfurization was performed with dibenzothiophene (DBT). In a typical case, the DBT (0.0735g, 0.4mmol) and the catalyst (0.075mmol) were added to 5 mL  $CH_2Cl_2$  and stirred for 10 min. Then, TBHP (2 mmol) were added to above mixture and heated at 50 °C for 3-7 h. An aliquot of the mixture was periodically removed and put into an ice chamber to stop the reaction. The identity of the product was ascertained by FT/IR and GC-MS, while the yield was obtained by HPLC analysis with a UV-Vis detector at  $\lambda = 254$  nm using an Inertsil SIL-100A C18 column. All analyses were performed with the mobile phase:  $CH_3CN:H_2O = 90:10$  at an operating flow rate of 1 mL  $min^{-1}$ . After the reaction, the catalyst was recovered by centrifugation, washed with distilled water and anhydrous ethanol alternately, and then dried in an oven at 60 °C for 24 h.

Model oil was obtained by dissolving desired amount of dibenzothiophene (DBT) in *n*-octane with a corresponding S-content of 500ppm, respectively. oxidation of dibenzothiophene in fuels were carried out by mixing 0.075mmol of nanocrystalline compound 2 and 5ml model oil in a two-necked kettle equipped with a magnetic stirrer and a condenser. After then, a desired amount of TBHP was rapidly added into the above mixture under vigorous stirring at 50°C. After the reaction, the residual sulfur content was removed by a polar extractant (for example, acetonitrile or 1-methyl-2-pyrrolidone), and monitored via HPLC analysis.

### X-ray crystallography

Single-crystal X-ray diffraction data for compounds 1-3 were recorded by using a Bruker Smart Apex CCD diffractometer with  $MoK_{\alpha}$  radiation ( $\lambda = 0.71073$  Å) at the temperature of 298(2) K. All structures were solved by the direct method and refined by a full-matrix least-squares method on  $F^2$  using the SHELXTL-97 crystallographic software package.<sup>16</sup> All non-hydrogen atoms were refined anisotropically, except for the lattice water molecules. The hydrogen atoms on organic carbon atoms were fixed in calculated positions. Hydrogen atoms on water molecules cannot be assigned from the weak reflection peaks but were directly included into the final molecular formula. During the refinement of compound 3, a number of O atoms on the polyoxoanion are disordered in two positions with 50% occupancy for each. Furthermore, the restraint command "ISOR" was used to restrain non-H atoms with ADP and NDP problems in compounds 1-3. Moreover, the triazole and benzene rings of the BBTZ ligands in all three compounds were also restrained with the commands "AFIX 69", "AFIX 59", "DELU", and "DFIX" so as to restrain the

bond distance and angles of organic ligands with a chemically reasonable structural features. All above restrained refinements led to relatively high restraint values of 229, 270 and 1212 for compounds **1-3**, respectively. In the final refinement, compound **2** exhibits solvent accessible voids but only three lattice water molecules can be clearly assigned from the residual peaks. Thus, the SQUEEZE program was further used to remove the contributions of disordered moieties from all of the observed structure factors.<sup>17</sup> The new generated hkl file was further used to refine the final crystal data. Based on

the elemental analysis, TG analysis and the SQUEEZE calculation result, another one water molecule is directly included in the final molecular formula of compound **2**. Crystal data and structural refinement for **1-3** are listed in Table 1. Selected bond lengths and angles of **1-3** are listed in Table S1- S3†. Crystallographic data for this paper has been deposited at the Cambridge Crystallographic Data Center: CCDC 1063971 for **1**, 1063960 for **2**, 1401904 for **3**. These data can be obtained free of charge from the Cambridge Crystallographic Data Centre via [www.ccdc.cam.ac.uk/data\\_request/cif](http://www.ccdc.cam.ac.uk/data_request/cif).

**Table 1.** Crystal data and structure refinement for **1-3**.

Compounds	1	2	3
Formula	C <sub>30</sub> H <sub>37</sub> N <sub>15</sub> O <sub>43</sub> PW <sub>12</sub> Co	C <sub>48</sub> H <sub>60</sub> N <sub>24</sub> O <sub>46</sub> BW <sub>12</sub> Co <sub>2.5</sub>	C <sub>120</sub> H <sub>128</sub> N <sub>60</sub> O <sub>84</sub> B <sub>2</sub> W <sub>24</sub> Cu <sub>5</sub>
Mr	3591.85	4073.53	8506.54
T / K	298(2)	298(2)	298(2)
Cryst. Syst.	Monoclinic	Triclinic	Monoclinic
Space group	C2/c	P-1	C2/c
a/Å	39.245(8)	11.7046(9)	51.260(4)
b/Å	15.242(3)	14.5353(11)	15.4783(10)
c/Å	23.514(5)	28.585(2)	24.3771(16)
α/°	90	85.5140(10)	90
β/°	115.77(3)	78.9940(10)	103.921(2)
γ/°	90	66.8170(10)	90
V/Å <sup>3</sup>	12666(4)	4388.3(6)	18773(2)
Z	8	2	4
μ / mm <sup>-1</sup>	22.086	16.215	15.292
F(000)	12768	3689	15484
Refls	10932	15268	16535
R <sub>int</sub>	0.0868	0.0322	0.0560
GOF	1.022	1.026	1.024
R <sub>1</sub> [I > 2σ(I)] <sup>a</sup>	0.0459	0.0420	0.0866
wR <sub>2</sub> (all data) <sup>b</sup>	0.0986	0.1011	0.1822

Note: <sup>a</sup>R<sub>1</sub> = Σ||F<sub>o</sub> - |F<sub>c</sub>||/Σ|F<sub>o</sub>|; <sup>b</sup>wR<sub>2</sub> = Σ[w(F<sub>o</sub><sup>2</sup> - F<sub>c</sub><sup>2</sup>)<sup>2</sup>]/Σ[w(F<sub>o</sub><sup>2</sup>)<sup>1/2</sup>].

## Results and discussion

### Crystal Structure of **1**

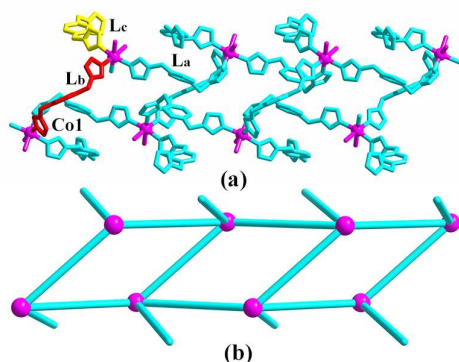


**Fig. 1** (a) Ball-and-stick and (b) schematic views of 1-D ladder-like chain unit in **1** formed by one Co<sup>2+</sup> center and BBTZ ligands with three different kinds of structural configurations.

Single-crystal X-ray diffraction analysis revealed compound **1** crystallizes in the monoclinic space group C2/c, and the crystallographically asymmetric unit consists of one polyoxoanion [PW<sub>12</sub>O<sub>40</sub>]<sup>3-</sup>, one Co<sup>2+</sup> (Co1) ion, one BBTZ bridging ligand and one monoprotonated HBBTZ ligand in general positions, another half BBTZ ligand lying about a twofold axis, two coordinated water molecules connected to Co1 center, and one lattice water molecule (Fig. 1, 2 and Fig. S1†). The cationic metal-organic fragment [Co(BBTZ)<sub>1.5</sub>(HBBTZ)(H<sub>2</sub>O)<sub>2</sub>]<sup>3+</sup> contains one crystallographically independent Co<sup>2+</sup> center, which adopts a six-coordinated mode with four nitrogen atoms derived from four BBTZ ligands and two coordinated water molecules (Fig. S1†). The bond lengths of Co–N range from 2.087(2) to 2.232(2) Å and the N–Co–N bond angles vary from 91.0(7) to 169.0(6)°. The bond distances of Co–O are in the range of 2.095(1) - 2.097(1) Å. It is noteworthy

that the BBTZ ligands in this metal-organic cationic moiety can be divided into three groups which are labeled with  $L_a$ ,  $L_b$  and  $L_c$  (Fig. 1a and Fig. S2†). The first group ( $L_a$ ) adopts *trans*-configuration and links adjacent two Co atoms into 1-D chains; The second group ( $L_b$ ) possesses *cis*-configuration and can be viewed as the “middle rail” that connects the adjacent 1-D chains to form a ladder-like chain; The third group ( $L_c$ ) displays *cis*-configuration and acts as “dangling arm”, protruding upper and lower sides of the ladder. It is noteworthy that the third group ( $L_c$ ) is monoprotonated and only one triazole group coordinate

with the Co center. In the packing arrangement, the adjacent 1-D chains are hydrogen-bonded by the lattice water molecules ( $O3w$ ), forming a porous 2-D supramolecular network on the *bc* plane (Fig. 2a and 2b and Fig. S3†). The guest Keggin-type POM anions and lattice water molecules are encapsulated in these voids (Fig. 2). Furthermore, the adjacent POM-encapsulated 2-D supramolecular networks are parallel with each other on the *bc* plane, and stack into 3-D supramolecular frameworks (Fig. 2c and 2d).

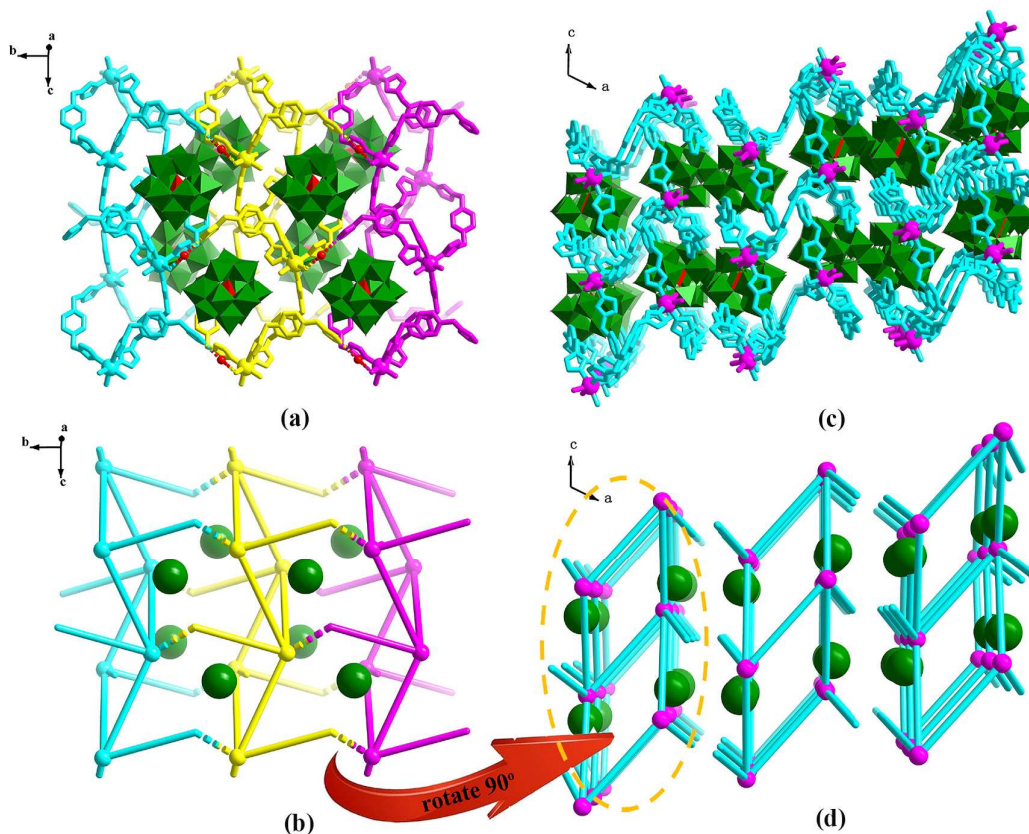


**Fig. 2** (a) POM-encapsulated 2-D supramolecular network in **1** viewed along *a* axis. 1-D ladder-like chains are shown with yellow, blue and purple color for clarity. The lattice water molecules are shown with red ball. POM units are shown with green polyhedra. (b) Schematic view of the 2-D supramolecular network topology in **1** viewed along *a* axis; (c) Polyhedral and ball-and-stick and (d) Schematic view of the 3-D POM-encapsulated supramolecular network of **1** viewed along *b* axis.

### Crystal Structure of **2**

Compound **2** crystallizes in the triclinic space group *P*-1 and the crystallographically asymmetric unit contains one Keggin-type polyoxoanion  $[BW_{12}O_{40}]^{5-}$ , two and half  $Co^{2+}$  (Co1, Co2, Co3) ions connected to the polyoxoanion, four BBTZ bridging ligands, two coordinated water molecules and four lattice water molecules (Fig. 3, Fig. 4 and Fig. S4†). In **2**, the Co3 atom lies on an inversion center, two BBTZ ligands lies in general positions while the other two lie about independent inversion centers. In **2**, there are two types of metal-organic coordination polymer fragments, that is, the 1-D chain and 2-D network (Fig. 3). The metal-organic 1-D chain possesses two crystallographically independent Co centers (Co1, Co2), which are hexa-

coordinated with three N atoms derived from three BBTZ ligands, two O atoms derived from two polyoxoanions, and one coordinated water molecule (Fig. 3a, 3b and Fig. S4†). The bond distances of Co-N and Co-O are in the range of 2.094(6) - 2.136(6) Å and 2.067(8) - 2.173(9) Å, respectively. The bond angles of N(O)-Co-N(O) are in the range of 82.5(4)° - 175.5(3)°. In the 1-D chain of compound **2**, adjacent Co(1) ions are connected by the *cis*-BBTZ bridging ligands ( $L_a$ ) to form a 1-D Co(1)-BBTZ chain (Fig. 3a). The adjacent Co(2) ion are linked by the *trans*-BBTZ ligands ( $L_b$ ) to form a 1-D zig-zag Co(2)-BBTZ chain (Fig. 3a). Meanwhile, another *trans*-BBTZ ligands ( $L_c$ ) bridge two Co(1)-BBTZ chains and one zig-zag Co(2)-BBTZ chain together to generate an unusual 1-D metal-organic chains with the “N”-type cross-section

viewed along *a* axis (Fig. S5†). The metal-organic 2-D network possesses one crystallographically independent Co center (Co3), which is hexa-coordinated with four N atoms derived from four BBTZ ligands and two O atoms derived from the two POM units (Fig. 4c and Fig. S4†). The bond lengths of Co(3)-N are in the range of 2.109(6) - 2.117(6) Å and the bond length of Co(3)-O is 2.148(8) Å. The bond angles of N(O)-Co-N(O) are in the range of 87.4(3)° - 180°. In such 2-D network, all BBTZ ligands possess similar structural *trans*-configurations and link the Co(3) centers into 2-D network with 4<sup>4</sup> *sqp* topology (Fig. 3c and 3d). Each mesh is large with the size of 11.70(5) × 26.72(5) Å (Fig. S6†). In compound **2**, the cationic metal-organic 1-D chains and 2-D networks are connected by the Keggin-type polyoxoanions to form a POM-supported 3-D framework (Fig. 4 and Fig. S8†). From the topological viewpoint, POM units can be viewed as a five-connected node, the Co(1) and Co(2) centers can be reduced to five-connected nodes, and Co(3) can be regarded as a six-connected node (Fig. S7†). Thus, the whole framework adopts the 4-nodal 5,5,5,6-c net with stoichiometry (5-c)<sub>2</sub>(5-c)<sub>2</sub>(5-c)<sub>2</sub>(6-c), and the point symbol for the net is {3.4<sup>3</sup>.5<sup>2</sup>.6<sup>4</sup>}<sub>2</sub>{3<sup>2</sup>.4.5<sup>4</sup>.6<sup>3</sup>}<sub>2</sub>{4<sup>4</sup>.5<sup>4</sup>.6<sup>2</sup>}<sub>2</sub>{4<sup>4</sup>.6<sup>10</sup>.8} (Fig. 4b).

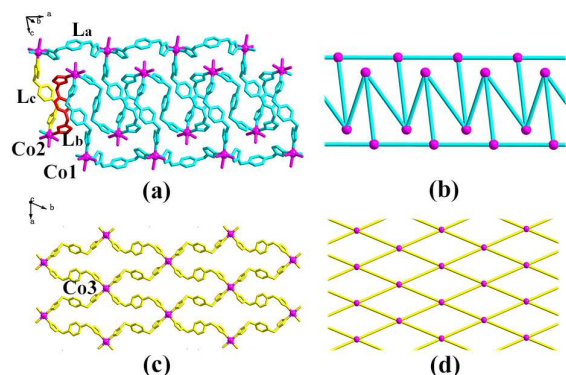


**Fig. 3** (a) Ball-and-stick and (b) schematic views of 1-D chainlike unit in **2**; (c) Ball-and-stick and (d) schematic views of 2-D network moiety in **2**.

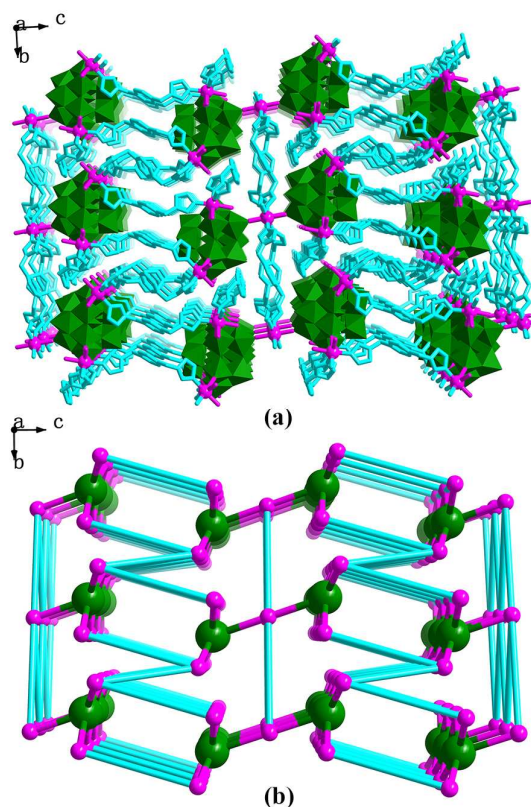


**Fig. 4** (a) Polyhedral and ball-and-stick and (b) schematic views of the POM-supported 3-D network of **2** viewed along *a* axis.

### Crystal Structure of **3**

Compound **3** crystallizes in the monoclinic space group *C2/c* and the crystallographically asymmetric unit consists of one Keggin-type polyoxoanion [BW<sub>12</sub>O<sub>40</sub>]<sup>5-</sup>, two and half Cu<sup>2+</sup> ions (Cu1, Cu2, Cu3) connected to the polyoxoanion, five BBTZ bridging ligands and two lattice water molecules (Fig. S9†). It is also worth noting that the Cu2 center lies on a twofold axis, three BBTZ ligands lie in general positions and two half BBTZ ligands lie about independent inversion centers. In **3**, three crystallographically independent Cu centers are all hexa-coordinated with four N atoms derived from four BBTZ ligands and two O atoms derived from two different POM units (Fig. 5, Fig. S9-S10†). The bond lengths of Cu-N and Cu-O are range from 2.004(1) – 2.08(2) Å and 2.211(1) – 2.791(1) Å, respectively. The five BBTZ ligands exhibit two types of structural configurations (Fig. S9†), that is, two *cis*-BBTZ ligands connect the Cu1 and Cu3 centers, while three *trans*-BBTZ ligands connect the Cu1-Cu3 centers, Cu1-Cu2 centers, Cu2-Cu2 centers and Cu3-Cu3 (generated by symmetry operations) centers, respectively. From the topological viewpoint, all three Cu centers can be reduced to a four-connection node. Thus, the whole cationic metal-organic framework adopt the 3-nodal 4,4,4-c net with stoichiometry (4-c)<sub>2</sub>(4-c)(4-c)<sub>2</sub>, and the point symbol for the net is {6<sup>3</sup>.7<sup>2</sup>.8}<sub>2</sub>{6<sup>6</sup>}<sub>2</sub>{7<sup>4</sup>.8<sup>2</sup>} (Fig. 5b). In such a cationic MOF framework, each guest Keggin-

type POM unit also connect with five Cu centers via the Cu-O bonds, further stabilizing the whole framework. Thus, if the POM unit can be reduced to a five-connectin node, the whole framework shall adopt the 4-nodal 5,6,6,6-c net with stoichiometry  $(5-c)_2(6-c)_2(6-c)(6-c)_2$ , and the point symbol for the net is  $\{3^2.4^3.5^4.6^6\}_2\{3^2.4^4.5^4\}_2\{3^2.4^5.5^5.6^2.7\}_2\{4^2.5^4.6^8.7\}$  (Fig. 6).

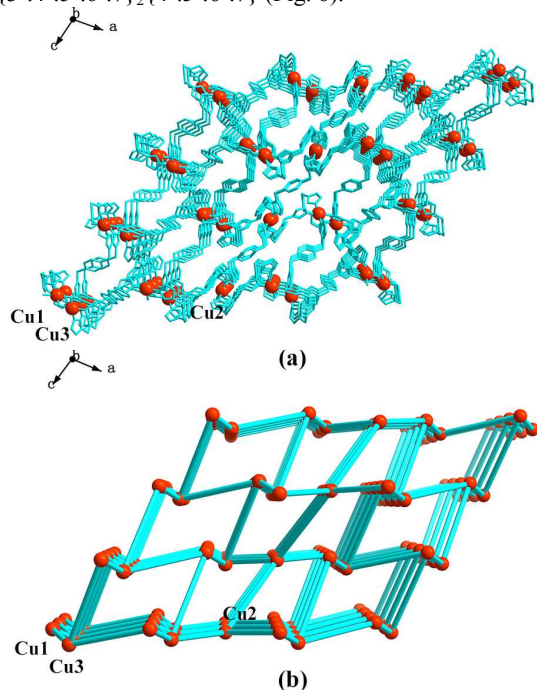


Fig. 5 (a) Ball-and-stick and (b) schematic views of the 3-D metal-organic network in **3**.

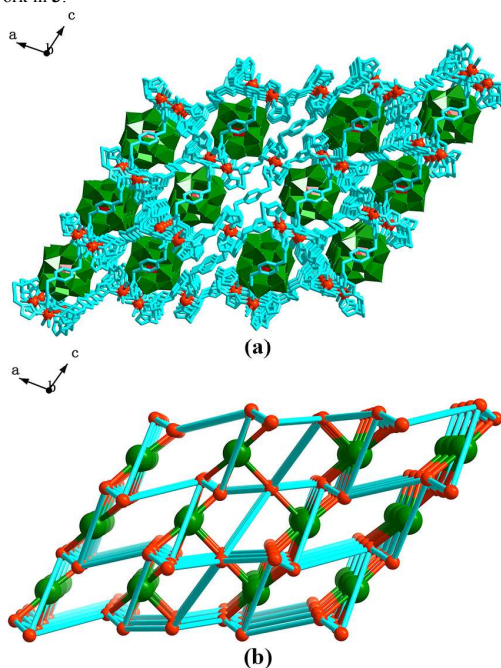
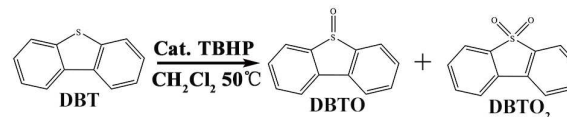


Fig. 6 (a) the chemical and (b) schematic view of the POM-supported 3-D open framework in **3**.

## Catalytic Oxidative Desulfurization

The desulfurization of fossil fuels is one of currently significant tasks, since their combustion waste can lead to serious atmospheric pollution, equipment corrosion and respiratory problems. In this research field, oxidative desulfurization has been developed an effective approach to remove the refractory organosulfur compounds by the catalytic oxidation into corresponding sulfoxes under mild reactions.<sup>17-22</sup> During the research process, dibenzothiophene (DBT) is usually employed as a typical refractory sulfur compound in fuel to evaluate the catalytic activities of test catalysts. In this case, the catalytic oxidation experiments of DBT with compounds **1-3** and a group of contrast catalysts were performed in  $\text{CH}_2\text{Cl}_2$  medium at 50 °C by using *tert*-butyl hydroperoxide (TBHP) as the oxidant (Scheme 2 and Table 2). The corresponding oxidized products were confirmed by FT/IR spectroscopy and GC-MS (Fig. S13 to S15†).



Scheme 2 Oxidation reaction of sulfide to corresponding sulfoxides and sulfones.

As shown in Fig. 7 and Table 2, compounds **1-3** all exhibit good catalytic activity on the oxidation of DBT into sulfoxide and sulfone. The maximum conversions can be observed after 7 h with the values of 91.57% for **1**, 99.63% for **2** and 96.68% for **3**, respectively, which are much higher than the conversion of 12.23 % in the contrast group (without catalyst). As shown in table S4, † compared with previous POM-based MOCNs catalysts, the catalytic activity of these three compounds have been improved remarkably. In order to explore the catalytic active moieties of compounds **1-3**, the catalytic activities of the precursors of compounds **1-3** were performed (see entry **5-12** in Table 2). It is found that the POM precursors exhibit obviously higher catalytic activity than those of TM precursors (Fig. S16†). Thus, POM units should be the catalytically active species in the composite coordination networks. This result is consistent with the reported catalytic mechanism of POM species. The Mo/W centers of POMs may activate and/or “capture” the peroxy groups, forming peroxy-POM intermediates, which can oxidize sulfide into sulfoxide and/or sulfone. During the oxidative process, the peroxy-POM species is transferred into POM species again and enter into next catalytic cycle.<sup>[19,20]</sup>

It is also noteworthy that the catalytic activities of compounds **1-3** are much higher than those of  $\text{H}_3\text{PW}_{12}\text{O}_{40}$  and  $\text{K}_5\text{BW}_{12}\text{O}_{40}$  POM salts (entry **5-6** in Table 2 and Fig. 7), indicating that the uniform dispersion of POM units into the metal-organic coordination networks in **1-3** at the molecular level may expose more POMs active sites, and thus remarkably improve the catalytic activities of the catalysts.

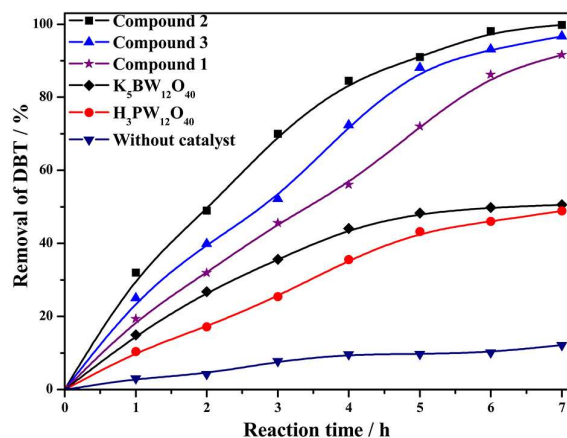


Fig. 7 Removal of DBT verse reaction time with different catalysts.

Table 2 Catalytic oxidation of sulfide to sulfoxide and sulfone with TBHP [a]

Entry	Catalyst	Time /h	Conversion% <sup>[c]</sup>
1	Compound 1	7	91.57
2	Compound 2	7	99.63
3	Nanocrystal compound 2	3	99.74
4	Compound 3	7	96.68
5	H <sub>3</sub> PW <sub>12</sub> O <sub>40</sub> ·n H <sub>2</sub> O	7	48.94
6	K <sub>5</sub> BW <sub>12</sub> O <sub>40</sub> ·n H <sub>2</sub> O	7	50.61
7	Co(OAc) <sub>2</sub> ·4H <sub>2</sub> O	7	25.26
8	Cu(OAc) <sub>2</sub> ·H <sub>2</sub> O	7	23.03
9	K <sub>5</sub> BW <sub>12</sub> O <sub>40</sub> ·n H <sub>2</sub> O, Co(OAc) <sub>2</sub> ·4H <sub>2</sub> O <sup>[b]</sup>	7	65.39
10	K <sub>5</sub> BW <sub>12</sub> O <sub>40</sub> ·n H <sub>2</sub> O, Cu(OAc) <sub>2</sub> ·H <sub>2</sub> O <sup>[b]</sup>	7	62.82
11	H <sub>3</sub> PW <sub>12</sub> O <sub>40</sub> ·n H <sub>2</sub> O, Co(OAc) <sub>2</sub> ·4H <sub>2</sub> O <sup>[b]</sup>	7	63.79
12	None	7	12.23

[a] Conditions: a mixture of catalyst (0.075 mmol), DBT (0.4 mmol), and TBHP (2.0 mmol, 5 equiv.) in CH<sub>2</sub>Cl<sub>2</sub> (2 mL) was stirred at 50°C. [b] Both POM and TM salts catalysts are 0.075 mmol. [c] The values are based on HPLC analysis.

As shown in Fig. 7, the catalytic activity of K<sub>5</sub>BW<sub>12</sub>O<sub>40</sub> is slight higher than that of H<sub>3</sub>PW<sub>12</sub>O<sub>40</sub>. Therefore, the catalytic activities of compounds 1-3 are slightly different with the order of 2 (99.63%) > 3 (96.68%) > 1 (91.57%). These catalytic differences between compound 1 and 2-3 may mainly derive from their difference of POM species. As a result of crystal structures, the loading amount of POMs in MOCNs of 2-3 is 70.13 % and 67.17 %, respectively. So the tiny catalytic difference between compound 2 and 3 is probably due to the loading amount of POM units, the different TM ions in the compounds (see entry 7-11 in Table 2) and the different network structural features of two compounds. Especially the last difference can be found from the powder X-ray diffraction patterns

(PXRD). Generally, the strong diffraction peaks of PXRD exhibit the advantage facets orientation of the crystalline compounds. In this case, the advantage facets {002} of compound 2 expose more POM units than the advantage facets {-111} of compound 3 (see Fig. S17†), suggesting that the advantage facets containing more POM units may be an important factor to effect the activity of catalysts.

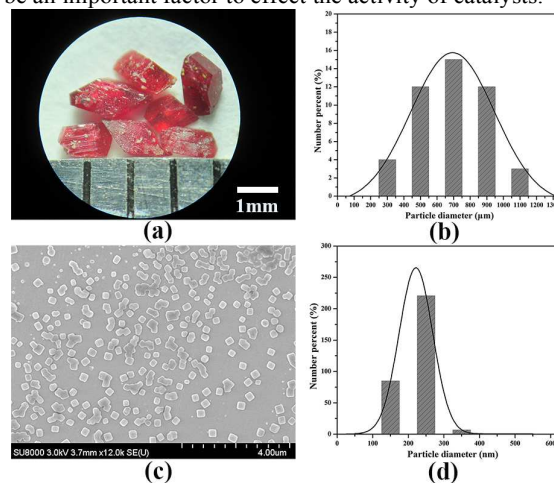


Fig. 8 (a) The images of single crystals 2 with the scale bar of 1mm; (b) the particle size distribution of single crystals 2; (c) the SEM image of nanocrystals 2; (d) the particle size distribution of nanocrystals 2.

Another possible route to improve the catalytic property of these hybrid catalysts is reducing the size of such crystalline catalysts, which can increase their specific surface area and expose more POM active sites during the catalytic process. In this case, the best efficient catalyst compound 2 is used as the representative sample to prepare the nano-crystallines. In this research field, the surfactant-assisted method has already been explored as an effective way to prepare nanoscale MOF materials, since the suitable surfactants can strongly influence the size of crystals and control the nucleation rate for the production highly crystalline materials.<sup>23-29</sup> Up to date, the nanocrystallines of POM-based MOCNs prepared by this surfactant-assisted hydrothermal synthesis method have not been reported yet. During the preparation, the key factor is to choose suitable surfactants. Herein, we successfully prepared the nanocrystalline compound 2 by the use of anionic surfactant sodium dodecyl sulfate (SDS).<sup>30-33</sup> SEM images show that uniform crystals are rectangle morphology with the size of about 245 nm in diameter (Fig. 8). The powder X-ray diffraction (PXRD) pattern and EDAX of nanocrystal 2 are same as those of the large single-crystal 2, confirming the structural consistence (Fig. S19 and S23†).

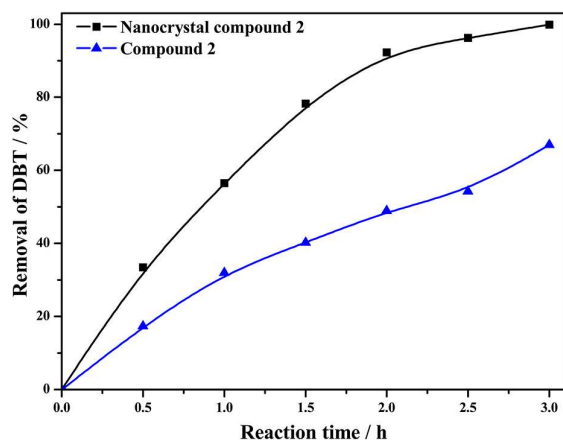


Fig. 9 Removal of DBT versus Reaction time.

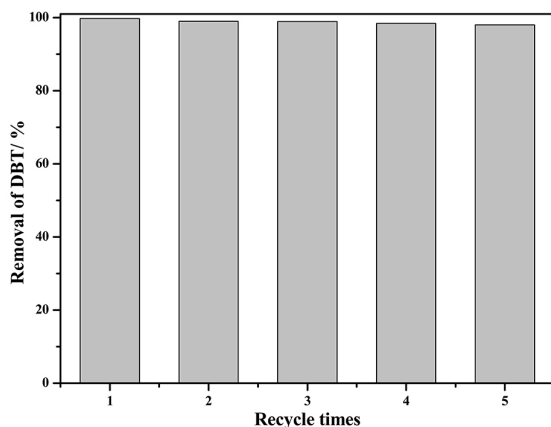


Fig. 10 The recycle experiments with nanocrystal 2 as catalyst.

The catalytic activity of nanocrystal 2 was studied in the same condition. It is observed that the conversion of DBT can almost reach 100 % after 3 h, indicating that the crystal size of the catalyst has effect on the catalytic activity (Fig. 9) obviously. When the crystal size of the catalyst 2 decreases, the specific surface area of catalysts is dramatically improved, thus more POM active sites were exposed, leading to high catalytic activity. In such catalytic reaction system, the nanocrystal 2 is insoluble and can be easily recycled by simple centrifugal separation (Fig. S18†). Recycling experiments reveal that the catalytic activity of the catalyst shows just slight decrease after reused for five cycles (Fig. 10), which might be related to the slight loss of catalyst in the process of recycle. The FT/IR spectra, UV-vis diffuse reflectance spectra and PXRD patterns (Fig. 11) of nanocrystal 2 before and after five catalytic cycles (Fig. 11, Fig. S19-S21†) show negligible change, suggesting that the nanocrystal 2 is stable in such catalytic reaction system. In order to simulate the oxidative desulfurization in fossil oil, the catalytic activity of nanocrystal 2 in the model oil *n*-octane was also studied. The conversion of DBT can reach 100% after 3 h (Fig. S34), manifesting that the nanocrystal 2 displayed excellent catalytic activity. The recycling experiments of

nanocrystal 2 in *n*-octane also have been investigated and the conversion of DBT still reached 96.3% after 5-times recycling without a significant decrease (Fig. S35).

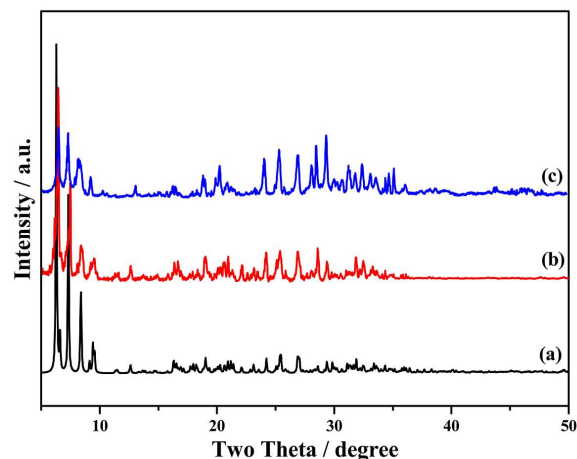


Fig. 11 PXRD patterns of nanocrystal 2 in  $2\theta$  range of 5 – 50° (a) simulated pattern; (b) as-synthesized sample of nanocrystal 2; (c) nanocrystal 2 after catalytic reaction.

## Conclusions

In summary, we presented three new Keggin-type POM-based metal-organic coordination networks. Compound 1 exhibits a POM-encapsulated 3-D supramolecular network, while compound 2 and 3 display the POM-supported 3-D coordination networks. All three compounds exhibited good catalytic activities in the heterogeneous catalytic oxidation desulfurization of DBT in contrast to their precursor POM salts, indicating that the mono-dispersion of POMs units in the metal-organic coordination networks at the molecular level can expose more active POM sites and increase the catalytic activity of the POM-based crystalline catalysts. In such non-porous POMs-based MOCN catalysts, a series of factors such as the POMs species, transition metal cations, the loading amount of POMs, and the structural features, can affect their catalytic activities and POM species is the main affecting factor. In order to further improve the catalytic activities of such type of catalysts, a new surfactant-assisted hydrothermal method for the preparation of nanocrystalline products has been developed. The uniform nanocrystals 2 were successfully prepared, which exhibits much better catalytic activity than the one of the large single crystal 2. This result confirm that reducing the size of crystalline catalysts can increase the specific surface area, expose more POM active sites, and thus improve the catalytic activity of the crystalline catalysts. This work confirms that the non-porous POM-based MOCNs can also be used as the heterogeneous catalysts for the oxidative desulfurization and the preparation of uniform nanocrystalline POM-based MOCN products may pave new ways to explore such heterogeneous POM-based catalysts with high efficient catalytic activity. This work is still ongoing in our research team.

## Acknowledgements

The authors gratefully acknowledge the financial support National Natural Science Foundation of China (grant nos. 21271039, 21201032, 21471028 and 21401131), Program for New Century Excellent Talents in University (grant no. NCET120813) and Fundamental Research Funds for the Central Universities (grant no. 11SSXT140).

## Notes and references

<sup>a</sup> Key Laboratory of Polyoxometalate Science of Ministry of Education Faculty of Chemistry, Northeast Normal University, Changchun, 130024, P.R. China.

E-mail: tanhq870@nenu.edu.cn (H.-Q. Tan) and liyg658@nenu.edu.cn (Y.-G. Li)

<sup>b</sup> School of Chemical and Biological Engineering, Taiyuan University of Science and Technology, Taiyuan, 030021, P.R. China.

E-mail: Haoxiuli1@163.com

<sup>c</sup> College of Science, Shenyang Agricultural University, Shenyang, 110866, P.R. China.

† Electronic Supplementary Information (ESI) available: Summary of selected bond lengths and angles; catalytic experiment data; IR, TG and PXRD and cif files of **1-3**. CCDC reference numbers: 871528 (**1**), 871529 (**2**), and 871981 (**3**). See DOI: 10.1039/b000000x/

- (a) T. V. Choudhary, J. Malandra, J. Green, S. Parrott, B. Johnson, *Angew. Chem. Int. Ed.*, 2006, **45**, 3299; (b) A. Nisar, J. Zhuang, X. Wang, *Adv. Mater.*, 2011, **23**, 1130; (c) Z. Guo, B. Liu, Q. H. Zhang, W. P. Deng, Y. Wang, Y. H. Yang, *Chem. Soc. Rev.*, 2014, **43**, 3480; (d) O. Reimann, C. Smet-Nocca, C. P. R. Hackenberger, *Angew. Chem. Int. Ed.*, 2015, **54**, 306; (e) W. S. Zhu, C. Wang, H. P. Li, P. W. Wu, S. H. Xun, W. Jiang, Z. G. Chen, Z. Zhao, H. M. Li, *Green Chem.*, 2015, **17**, 2464; (f) W. W. He, G. S. Yang, Y. J. Tang, S. L. Li, S. R. Zhang, Z. M. Su, Y. Q. Lan, *Chem. Eur. J.*, 2015, **21**, 1.
- (a) H. Y. Lü, J. B. Gao, Z. X. Jiang, Y. X. Yang, B. Song, C. Li, *Chem. Commun.*, 2007, 150; (b) S. Ribeiro, C. M. Granadeiro, P. Silva, F. A. Almeida Paz, F. F. D. Biani, L. Cunha-Silva, S. S. Balula, *Catal. Sci. Technol.*, 2013, **3**, 2404.
- (a) S. G. Mitchell, C. Streb, H. N. Miras, T. Boyd, D. L. Long, L. Cronin, *Nat. Chem.*, 2010, **2**, 308; (b) P. Putaj, F. Lefebvre, *Coord. Chem. Rev.*, 2011, **255**, 1642; (c) P. Huang, C. Qin, Z. M. Su, Y. Xing, X. L. Wang, K. Z. Shao, Y. Q. Lan, E. B. Wang, *J. Am. Chem. Soc.*, 2012, **134**, 14004; (d) X. B. Han, Z. M. Zhang, T. Zhang, Y. G. Li, W. B. Lin, W. S. You, Z. M. Su, E. B. Wang, *J. Am. Chem. Soc.*, 2014, **136**, 5359; (e) X. B. Han, Y. G. Li, Z. M. Zhang, H. Q. Tan, Y. Lu, E. B. Wang, *J. Am. Chem. Soc.*, 2015, **137**, 5486.
- (a) N. Mizuno, K. Yamaguchi, K. Kamata, *Coord. Chem. Rev.*, 2005, **249**, 1944; (b) D. Huang, Y. J. Wang, L. M. Yang, G. S. Luo, *Ind. Eng. Chem. Res.*, 2006, **45**, 1880; (c) D. Julião, A. Gomes, M. Pillinger, L. Cunha-Silva, B. D. Castro, I. Gonçalves, S. S. Balula, *Fuel Process. Technol.*, 2015, **131**, 78; (d) J. X. Wu, W. Zhang, A. Tang, Y. L. Gao, Y. Y. Tan, Y. Men, B. H. J. Tang, *Inorg. Chim. Acta.*, 2015, **425**, 108.
- (a) B. Keita, D. Bouaziz, L. Nadjio, *J. Electrochem. Soc.*, 1988, **135**, 87; (b) S. J. Dong, X. D. Xi, M. Tian, *J. Electroanal. Chem.*, 1995, **385**, 227.
- (a) F. Bigi, A. Corradini, C. Quarantelli, G. Sartori, *J. Catal.*, 2007, **250**, 222; (b) K. Yazu, Y. Yamamoto, T. Furuya, K. Miki, K. Ukegawa, *Energy Fuels.*, 2001, **15**, 1535.
- (a) Y. Q. Lan, H. L. Jiang, S. L. Li, Q. Xu, *Adv. Mater.*, 2011, **23**, 5015; (b) C. Wang, K. E. deKrafft, W. B. Lin, *J. Am. Chem. Soc.*, 2012, **134**, 7211; (c) C. Y. Sun, X. L. Wang, X. Zhang, C. Qin, P. Li, Z. M. Su, D. X. Zhu, G. G. Shan, K. Z. Shao, H. Wu, J. Li, *Nat. Commun.*, 2013, **4**, 2717; (d) X. H. Liu, J. G. Ma, Z. Niu, G. M. Yang, P. Cheng, *Angew. Chem. Int. Ed.*, 2015, **54**, 988.
- (a) M. L. Wei, C. He, W. J. Hua, C. Y. Duan, S. H. Li, Q. J. Meng, *J. Am. Chem. Soc.*, 2006, **128**, 13318; (b) F. J. Ma, S. X. Liu, C. Y. Sun, D. D. Liang, G. J. Ren, F. Wei, Y. G. Chen, Z. M. Su, *J. Am. Chem. Soc.*, 2011, **133**, 4178; (c) H. Fu, C. Qin, Y. Lu, Z. M. Zhang, Y. G. Li, Z. M. Su, W. L. Li, E. B. Wang, *Angew. Chem. Int. Ed.*, 2012, **51**, 7985; (d) Z. M. Zhang, T. Zhang, C. Wang, Z. K. Lin, L. S. Long, W. B. Lin, *J. Am. Chem. Soc.*, 2015, **137**, 3197.
- (a) S. T. Zheng, J. Zhang, G. Y. Yang, *Angew. Chem. Int. Ed.*, 2008, **47**, 3909; (b) C. Y. Sun, S. X. Liu, D. D. Liang, K. Z. Shao, Y. H. Ren, Z. M. Su, *J. Am. Chem. Soc.*, 2009, **131**, 1883; (c) D. Y. Shi, C. He, B. Qi, C. Chen, J. Y. Niu, C. Y. Duan, *Chem. Sci.*, 2015, **6**, 1035.
- (a) R. Y. Hang, C. B. Du, S. J. Feng, C. L. Wang, Z. P. Kong, B. Yue, H. Y. He, *CrystEngComm.*, 2011, **13**, 7143.
- (a) S. X. Liu, L. H. Xie, B. Gao, C. D. Zhang, C. Y. Sun, D. H. Li, Z. M. Su, *Chem. Commun.*, 2005, 5023; (b) S. Yao, J. H. Yan, H. Duan, Z. M. Zhang, Y. G. Li, X. B. Han, J. Q. Shen, H. Fu, E. B. Wang, *Eur. J. Inorg. Chem.*, 2013, 4770; (c) S. B. Li, H. Y. Ma, H. J. Pang, L. Zhang, *Cryst. Growth Des.*, 2014, **14**, 4450.
- (a) D. Y. Du, J. S. Qin, S. L. Li, Z. M. Su, Y. Q. Lan, *Chem. Soc. Rev.*, 2014, **43**, 4615; (b) W. W. He, S. L. Li, H. Y. Zang, G. S. Yang, S. R. Zhang, Z. M. Su, Y. Q. Lan, *Coord. Chem. Rev.*, 2014, **279**, 141.
- (a) X. L. Hao, Y. Y. Ma, C. Zhang, Q. Wang, X. Cheng, Y. H. Wang, Y. G. Li, E. B. Wang, *CrystEngComm.*, 2012, **14**, 6573; (b) X. L. Hao, Y. Y. Ma, Y. H. Wang, L. Y. Xu, F. C. Liu, M. M. Zhang, Y. G. Li, *Chem. Asian. J.*, 2014, **9**, 819; (c) X. L. Hao, Y. Y. Ma, W. Z. Zhou, H. Y. Zang, Y. H. Wang, Y. G. Li, *Chem. Asian. J.*, 2014, **9**, 3633; (d) X. L. Hao, Y. Y. Ma, H. Y. Zang, Y. H. Wang, Y. G. Li, E. B. Wang, *Chem. Eur. J.*, 2015, **21**, 3778.
- X. R. Meng, Y. L. Song, H. W. Hou, H. Y. Han, B. Xiao, Y. T. Fan, Y. Zhu, *Inorg. Chem.*, 2004, **43**, 3528.
- R. D. Claude, F. Michel, F. Raymonde and T. Rene, *Inorg. Chem.*, 1983, **22**, 207.
- (a) G. M. Sheldrick, *SHELXS-97, Program for solution of crystal structures*, University of Göttingen, Germany, 1997; (b) G. M. Sheldrick, *SHELXL-97, Program for refinement of crystal structures*, University of Göttingen, Germany, 1997. (c) A. L. Spek, *Acta Cryst.*, 2009, **D65**, 148-155.
- Y. W. Liu, S. M. Liu, S. X. Liu, D. D. Liang, S. J. Li, Q. Tang, X. Q. Wang, J. Miao, Z. Shi, Z. P. Zheng, *ChemCatChem.*, 2013, **5**, 3086.
- N. Mizuno, K. Kamata, K. Yamaguchi, *catalysis Today.*, 2012, **185**, 157.
- (a) D. Liu, Y. Lu, H. Q. Tan, W. L. Chen, Z. M. Zhang, Y. G. Li, E. B. Wang, *Chem. Commun.*, 2013, **49**, 3673; (b) C. M. Granadeiro, A. D. S. Barbosa, S. Ribeiro, I. C. M. S. Santos, B. D. Castro, L. Cunha-Silva, S. S. Balula, *Catal. Sci. Technol.*, 2014, **4**, 1416; (c) M. Li, M. Zhang, A. M. Wei, W. S. Zhu, S. H. Xun, Y. N. Li, H. P. Li, H. M. Li, *J. Mol. Catal. A: Chem.*, 2015, **406**, 23; (d) S. H. Xun, W. S. Zhu, F. X. Zhu, Y. H. Chang, D. Zheng, Y. J. Qin, M. Zhang, W. Jiang, H. M. Li, *Chem. Eng. J.*, 2015, **280**, 256.
- (a) W. S. Zhu, W. L. Huang, H. M. Li, M. Zhang, W. Jiang, G. Y. Chen, C. R. Han, *Fuel Process. Technol.*, 2011, **91**, 1842; (b) Z. X. Zhang, F. W. Zhang, Q. Q. Zhu, W. Zhao, B. C. Ma, Y. Ding, *J. Colloid Interf. Sci.*, 2011, **360**, 189; (c) X. M. Yan, Z. K. Mei, P. Mei, Q. F. Yang, *J. Porous. Mat.*, 2014, **21**, 729; (d) H. Y. Lü, C. L. Deng, W. Z. Ren, X. Yang, *Fuel Process. Technol.*, 2014, **119**, 87; (e) L. S. Nogueira, S. Ribeiro, C. M. Granadeiro, E. Pereira, G. Feio, L. Cunha-Silva, S. S. Balula, *Dalton. Trans.*, 2014, **43**, 9518; (f) W. S. Zhu, B. L. Dai, P. W. Wu, Y. H. Chao, J. Xiong, S. H. Xun, H. P. Li, H. M. Li, *ACS Sustainable Chem. Eng.*, 2015, **3**, 186.
- (a) W. S. Zhu, H. M. Li, X. Jiang, Y. S. Yan, J. D. Lu, L. N. He, J. X. Xia, *Green Chem.*, 2008, **10**, 641; (b) H. Y. Lü, Y. N. Zhang, Z. X. Jiang, C. Li, *Green Chem.*, 2010, **12**, 1954.
- B. Y. Zhang, Z. X. Jiang, J. Li, Y. N. Zhang, F. Lin, Y. Liu, C. Li, *J. Catal.*, 2012, **287**, 5.
- (a) L. H. Wee, S. R. Bajpe, N. Janssens, I. Hermans, K. Houthoofd, C. E. A. Kirschhock, J. A. Martens, *Chem. Commun.*, 2010, **46**, 8186; (b) L. H. Wee, N. Janssens, S. R. Bajpe, C. E. A. Kirschhock, J. A. Martens, *Catal Today.*, 2011, **171**, 275; (c) D. D. Liang, S. X. Liu, F. J. Ma, F. Wei, Y. G. Chen, *Adv. Synth. Catal.*, 2011, **353**, 733.
- J. M. Yang, Q. Liu, Y. S. Kang, W. Y. Sun, *Dalton Trans.*, 2014, **43**, 16707.
- R. Narayanan, M. A. El-Sayed, *J. Phys. Chem. B.*, 2005, **109**, 12663.
- M. J. Rosen, S. B. Sulthana, *J. Colloid Interf. Sci.*, 2001, **239**, 528.
- F. Zaera, *Chem. Soc. Rev.*, 2013, **42**, 2746.
- M. Y. Ma, D. Zacher, X. N. Zhang, R. A. Fischer, N. Metzler-Nolte, *Cryst. Growth Des.*, 2011, **11**, 185.
- Z. Ni, R. I. Masel, *J. Am. Chem. Soc.*, 2006, **128**, 12394.
- A. Mirabi, A. S. Rad, H. Khodadad, *J. Magn. Magn. Mater.*, 2015, **389**, 130.

- 31 S. Hussain, T. M. Liu, N. Aslam, M. Kashif, S. X. Cao, M. Rashad, Y. Zhang, W. Zeng, M. S. Javed, *Mater Lett.*, 2015, **152**, 260.
- 32 X. X. Xu, X. Gao, T. T. Lu, X. X. Liu, X. L. Wang, *J. Mater. Chem. A.*, 2015, **3**, 198.
- 33 Y. J. Yang, A. V. Kelkar, X. L. Zhu, G. R. Bai, H. T. Ng, D. S. Corti, E. I. Franses, *J Colloid Interf Sci.*, 2015, **450**, 434.

## ARTICLE

## TOC:

Polyoxometalate-Based Metal-Organic Coordination Networks for Heterogeneous Catalytic Desulfurization.

